



ELSEVIER



<https://doi.org/10.1016/j.ultrasmedbio.2020.08.006>

## ● Original Contribution

# H-SCAN, SHEAR WAVE AND BIOLUMINESCENT ASSESSMENT OF THE PROGRESSION OF PANCREATIC CANCER METASTASES IN THE LIVER

JIHYE BAEK,\* RIFAT AHMED,\* JIAN YE,<sup>†</sup> SCOTT A. GERBER,<sup>†</sup>  
KEVIN J. PARKER,\* and MARVIN M. DOYLEY\*

\*Department of Electrical and Computer Engineering, University of Rochester, Rochester, New York, USA; and <sup>†</sup>Department of Surgery, University of Rochester Medical Center, Rochester, New York, USA

(Received 24 April 2020; revised 4 August 2020; in final form 5 August 2020)

**Abstract**—The non-invasive quantification of tumor burden and the response to therapies remain an important objective for imaging modalities. To characterize the performance of two newly optimized ultrasound-based analyses, we applied shear wave and H-scan scattering analyses to repeated trans-abdominal ultrasound scans of a murine model of metastatic pancreatic cancer. In addition, bioluminescence measurements were obtained as an alternative reference. The tumor metastases grow aggressively and result in death at approximately 4 wk if untreated, but longer for those treated with chemotherapy. We found that our three imaging methods (shear wave speed, H-scan, bioluminescence) trended toward increasing output measures with time during tumor growth, and these measures were delayed for the group receiving chemotherapy. The relative sensitivity of H-scan tracked closely with bioluminescence measurements, particularly in the early to mid-stages of tumor growth. The correlation between H-scan and bioluminescence was found to be strong, with a Spearman's rank correlation coefficient greater than 0.7 across the entire series. These preliminary results suggest that non-invasive ultrasound imaging analyses are capable of tracking the response of tumor models to therapeutic agents. (E-mail: [kevin.parker@rochester.edu](mailto:kevin.parker@rochester.edu)) © 2020 World Federation for Ultrasound in Medicine & Biology. All rights reserved.

**Key Words:** Molecular and cellular imaging, Ultrasound, Abdomen, Animal models and imaging, Liver, Quantification and estimation.

## INTRODUCTION

Measuring the extent of metastatic cancer in the liver is an important goal with relevance to assessing the effectiveness of therapies. Ultrasound has advantages over other modalities in being portable, widely accessible, non-ionizing and low cost. A number of advanced techniques have been applied to distinguish responders versus non-responders using ultrasound imaging (Tadayyon et al. 2016; Turco et al. 2016; Dizeux et al. 2017; Tadayyon 2017; Zhou et al. 2017; Fernandes et al. 2019; Khairalseed et al. 2019; Li et al. 2019; Sannachi et al. 2019). Also, with the emergence of advanced shear wave elasticity techniques, the stiffness or viscoelastic properties of tumors has been investigated (Parker et al. 2011; Chang et al. 2013; Barr et al. 2015). Recently, we assessed the progression

of a pancreatic ductal adenocarcinoma (PDAC) model (Ahmed et al. 2020) using bioluminescence measures and shear wave elastography (SWE). We demonstrated that SWE has a significant increase with tumor growth.

In this paper, we study the additional information gained from H-scan analysis. The H-scan is a matched filter approach that seeks to classify returning echoes from tissue according to their spectral content, corresponding to the size and shape of the inhomogeneous scattering sites (Parker 2016a; Parker 2016b; Parker and Baek 2020). The information can be coded as color hues and incorporated in the display so as to add a visual depiction of the matched filter output. We have chosen red colors to represent lower frequency and larger scatterers, while blue colors indicate smaller structures approaching the Rayleigh scattering regime. This red/blue color scheme also parallels the relative size of wavelengths of visible light. It has been found that the H-scan can be sensitive to subtle (on the order of 10 microns) shifts in scattering sizes using frequencies and

Address correspondence to: Kevin J. Parker, University of Rochester, Computer Studies Building, Box 270231, Rochester, New York 14627-0231. E-mail: [kevin.parker@rochester.edu](mailto:kevin.parker@rochester.edu)

bandwidths within the conventional human clinical ultrasound band (Khairalseed et al. 2017). Preliminary results on tumor models have shown sensitivity to cellular changes after administration of therapeutic agents (Khairalseed et al. 2019). In this study, we assess the H-scan methodology on a murine metastatic pancreatic tumor model as it grows in the liver. In addition, the results are compared with both SWE and bioluminescence imaging (BLI) techniques as independent measurements (Rehemtulla et al. 2000). H-scan and elastography measures are both presumed to be related to the structure and composition of the tissue; however, they have not been previously compared, and this study begins a parallel accounting of these complementary methods. Separately, the bioluminescent measures are related to genetic expression and are integrated across the field of view of the camera; therefore, this offers a sensitive measure of cellular growth and spread within a region proximal to the camera.

This paper is organized as follows: First, the three measurement methods are described as applied to a murine tumor model, then the results are given as a function of time during the growth of the tumor in treated and untreated groups. Cross-comparisons of the three measurements are made among and between treated and untreated groups. The three methods all trend toward increasing measures with increasing time of the growth and spread of the metastases; however, the sensitivity in early growth phases is not equal.

## METHODS

### *Experimental setup*

*Animal study.* All animal studies were performed under a protocol approved by the University of Rochester Committee on Animal Resources. We purchased the animals used in this study from Jackson Laboratory (Bar Harbor, ME, USA) (Soares et al. 2014) and maintained them in a pathogen-free facility on a standard diet and protocol as described in Mills et al. (2019). Ten female mice were enrolled, and  $4 \times 10^5$  luciferase-expressing murine pancreatic tumor cells (KCKO-luc) (Soares et al. 2014) were used to initiate the model. Mice were anesthetized using an isoflurane anesthetic vaporizer (Scivena Scientific, Clackamas, OR, USA), and a 10 mm laparotomy incision was made to expose the spleen and pancreas. We manually occluded a part of the spleen (hemispleen) and injected primary cancer cells in this region. After allowing time for the cells to diffuse into the liver *via* hepatic vein, this part of the spleen was surgically removed. Details of the protocol can be found in Soares et al. (2014) and Mills et al. (2019). These

were divided into two groups: A control group and an experimental group. Each group had five mice, and the mice in the experimental group were treated with chemotherapy: 50 mg/kg of gemcitabine was administered twice per wk by retro-orbital injection.

*B-scan data acquisition and processing.* The liver images of the 10 mice were acquired using a Verasonics ultrasound scanner (Vantage 256, Verasonics, Inc., Kirkland, WA, USA). Each scan used the L11-5v probe at a 10 MHz center frequency using compounded plane wave imaging (25 angles,  $-6^\circ$  to  $6^\circ$ ). The scans were repeated from 10 d from tumor injection up to their death. To set the region of interest (ROI), the liver of each image was manually contoured, which was used for H-scan, SWE and BLI. The plane wave B-scan radiofrequency (RF) data and ROI for liver were assigned as inputs for H-scan.

*SWE.* We also implemented the plane wave single track location shear wave elasticity imaging method on a research scanner (Vantage 256, Verasonics Inc.) using an L11-5v probe (Ahmed et al. 2018). We used a total of 41 push beams (0.3 mm apart) laterally spaced over a distance of 1.2 cm. Each push beam (5 MHz transmit) consisted of four rapid multifocal zones at depths of 10, 15, 20 and 25 mm and each focal zone push beam was 150 micro-seconds long (a total of 600 micro-seconds). After each push beam, shear waves were tracked using compounded plane wave imaging (10 MHz, angles of  $-1^\circ$ ,  $0^\circ$  and  $1^\circ$ ). Shear wave speed (SWS) was reconstructed by comparing arrival times of a pair of push beams separated by 0.9 mm at a common track location. The SWS for a given pair of push beams were also averaged over multiple track positions (Ahmed et al. 2018; Ahmed et al. 2020). Only the track lines within the body cavity of the animal were considered (Ahmed et al. 2020). A weighted averaging (weight: square of the normalized cross-correlation coefficient of wave pairs) was performed when combining multiple track line estimates.

*BLI.* Tumor growth in the liver was monitored over time using BLI independent of H-scan and elastography. A commercial system (IVIS Spectrum, PerkinElmer Inc., Waltham, MA, USA) was used to acquire bioluminescence images twice a week for 6 wk, within 24 h of B-scan and elastography. D-Luciferin 75 mg/kg was injected subcutaneously, and 12 min after the D-Luciferin injection, the mice were anesthetized with 3% isoflurane (Fluriso, VetOne, Boise, ID, USA). The average radiance (photons/sec/cm<sup>2</sup>/sr) was measured using the Living Image software (PerkinElmer Inc., Waltham, MA, USA).

## H-scan

The H-scan framework classifies the scatterer size using convolution of received echoes with a *matched filter* set including Gaussian-weighted Hermite functions or close relatives such as Gaussian bandpass functions. The convolution in time domain or bandpass filter in frequency domain can enhance specific frequency components in ultrasound B-scan depending on the specification of a used matched filter set. Gaussian functions with  $N_c$  different center frequencies correspond to  $N_c$  levels of colormap. For each pixel in B-scan, the maximum output among the  $N_c$  matched filters determines the color for the pixel; red and blue colors represent relatively larger and smaller scatterers, respectively. The schematic for H-scan is shown in Figure 1.

Before the H-scan process, attenuation correction was performed to compensate for the frequency down shift along with the depth. Frequency-dependent attenuation is a physical property of ultrasound propagation in a medium, which gradually shifts the H-scan color distribution from blue at near field to red at far field. To compensate for this, the axial direction of an input ultrasound image was divided into five zones, and the frequency spectra of each zone were compensated by  $e^{+\hat{\alpha}fx_z}$ , where  $x_z$  is the representative depth of each zone and  $\hat{\alpha}$  is the round-trip attenuation coefficient; 0.1 Np/cm/MHz was used for this study based on estimates of the decay (Parker and Waag 1983; Parker 1986; Parker 2019).

The attenuation corrected signal is assigned as an input of the matched filter processing; Gaussian functions were used as the matched filter. To obtain the  $N_c$  number of colormap levels,  $N_c$  Gaussian functions are required, whose center frequency is different but whose bandwidths are the same:  $N_c = 256$  for this study. The center frequencies of each Gaussian function were set ranging from 3.3–11.3 MHz, resulting in equally divided 256 center frequencies. Each filter had a  $\sigma$  of 2.0. These parameters were based on the early stage tumor echoes.

For the step of color processing, a colormap for H-scan is employed, as shown in the color bar of Figure 2a, to represent relative size of scatterers. The color distribution is chosen to illustrate the size difference effectively.

The H-scan color processing methodology assigns the peak frequency of the maximum matched filter output to a blue/red color scheme (Parker and Baek 2020). The convolution processing between the RF signal and the set of matched filters generates  $N_c$  convolution values for each sampling point of RF signal. This processing is also performed over all scanlines. Each point has one maximum among the  $N_c$  possible values, and is assigned an associated color as quantified in the following section.

As the last step of the H-scan procedure, B-scan and colormap images are combined as transparencies for display. By showing the blended image of B-scan and colormap images, the H-scan image can demonstrate spatial resolution and frequency resolution within one image at the same time; the B-scan shows high spatial resolution with black and white color, and the H-scan processing can represent spectral information for each pixel using colors from red to blue as a concept of a matched filter corresponding to shifts in the scattering transfer function (Parker 2016a; Khairalseed *et al.* 2017).

## Evaluation metric and statistical analysis

This study used specific measurements for each of the three methods employed: Intensity-weighted-percentage of blue ( $IWP_{\text{blue}}$ ), SWS, and radiance were used for H-scan, SWE, and BLI, respectively.  $IWP_{\text{blue}}$  and SWS were investigated within the manually segmented liver region. Radiance data are obtained from the abdominal region, as illustrated in Figure 2c.

As shown in eqn (1), the H-scan parameters  $IWP_{\text{blue}}$  and  $IWP_{\text{red}}$  are given by:

$$(IWP_{\text{blue}}) = \frac{\frac{1}{n_B} \sum_{i \in B} I_i}{\frac{1}{n_B} \sum_{i \in B} I_i + \frac{1}{n_R} \sum_{i \in R} I_i} \times 100\% \quad (1)$$

$$(IWP_{\text{red}}) = \frac{\frac{1}{n_R} \sum_{i \in R} I_i}{\frac{1}{n_B} \sum_{i \in B} I_i + \frac{1}{n_R} \sum_{i \in R} I_i} \times 100\%,$$

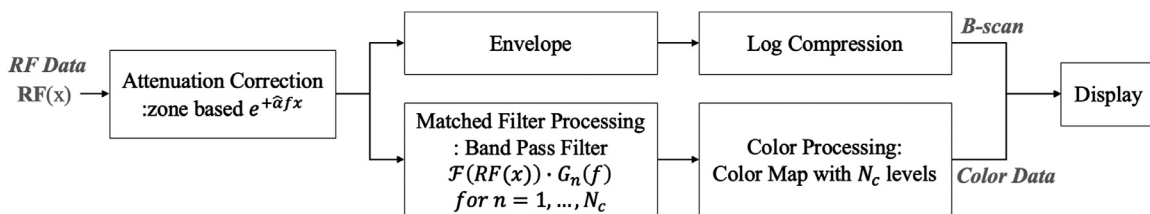


Fig. 1. Schematic for H-scan.

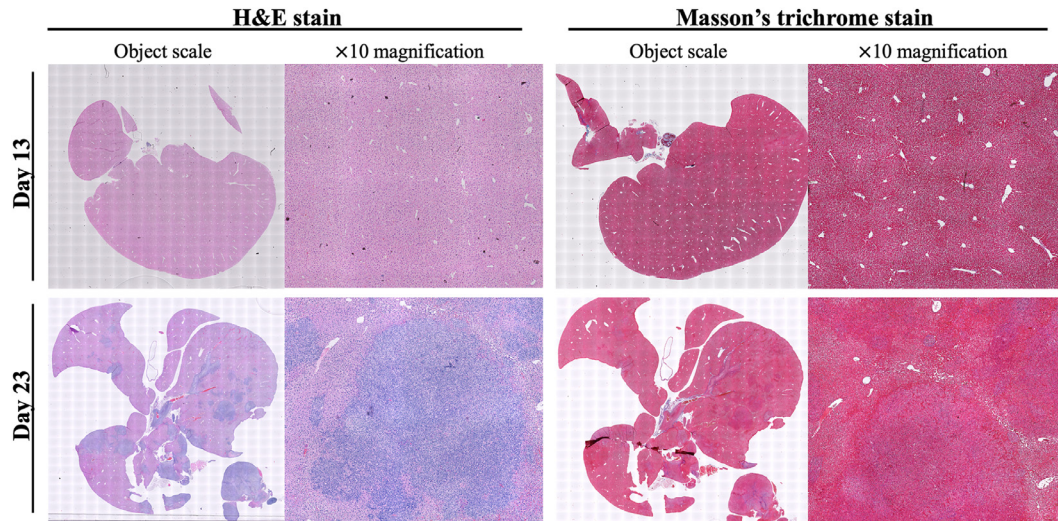


Fig. 2. Histology images from an untreated rat at early stage (day 13, top) and late stage (day 23, bottom), at scales of whole object and 10 $\times$  magnification. Left: Hematoxylin and eosin (H&E) stained sections, and right: Masson's trichrome stain. Pathologic changes can be seen between early and late stages as multiple metastatic lesions become distributed throughout the liver.

where  $i$  is index of each pixel in B-mode image,  $I_i$  is normalized color intensity for  $i$ ,  $I_i$  ranges from 0–1 and the number of blue and red pixels is given by  $n_B$  and  $n_R$ , respectively. The indices,  $i \in B$  and  $i \in R$ , are pixels classified as blue and red, respectively.  $I_i$  can be calculated from the H-scan colormap, which ranges from 1–256; the range of 1–128 represents red, and that of 129–256 represents blue. The color map data are normalized as  $I_i$  ranging from 0–1; the red colors from 128–1 are reassigned to 0–1 in sequence, and the blue colors from 129–256 are reassigned to 0–1. As shown in eqn (2), these are given by:

$$I_{i \in B} = \frac{C_1 - 129}{127}, \quad (2)$$

where  $C_1$  is the colormap for the  $i$ th pixel for blue data and

$$I_{i \in R} = \frac{128 - C_1}{127}, \quad (3)$$

for red data, as shown in eqn (3). For convenience,  $IWP_{\text{blue}}$  is simply called “% of blue” in this paper.

To compare the performance of the three different measurements, violin plots and Spearman's correlation ( $r_s$ ) were investigated. For the statistical analysis, analysis of variance with Tukey multiple comparison method was performed, resulting in  $p$  values.

## RESULTS

The PDAC metastases create an increasing tumor burden over time, typically in a pattern of individual lesions distributed throughout the liver, as shown in

Figure 2. To illustrate the image types collected by H-scan, SWE and BLI, the example images for the same mouse with tumor are shown in Figure 3; the fifth mouse in Figure 3c is the subject scanned for H-scan and SWE, shown in Figures 3a and 3b, respectively.

The measured parameters using H-scan, SWE and BLI over time are shown in Figure 4. To graph the different parameters onto a common scale and dynamic range, the relative scale values are calculated using simple linear translations of the raw data, as shown in eqn (4):

$$\begin{aligned} y_{Hscan} &= 1 \cdot Hscan_{org} + 0, \\ y_{SWE} &= 10 \cdot SWE_{org} + 30, \text{ and} \\ y_{BLI} &= 2.8 \cdot \log_e(BLI_{org}) + 10, \end{aligned} \quad (4)$$

where  $Hscan_{org}$ ,  $SWE_{org}$ , and  $BLI_{org}$  are the original raw data from the three methods;  $y_{Hscan}$ ,  $y_{SWE}$ , and  $y_{BLI}$  are relatively scaled values for the  $y$ -axis in Figure 4, and radiance measurements are traditionally reported on a log scale. The observed values of the three methods tend to increase as a tumor becomes more severe, until death.

The performance of H-scan is evaluated by the color images and by quantitative analysis. A total of ten mice including untreated and treated group were investigated using H-scan, of which representative image examples are shown in Figures 5 and 6, respectively. Over time, the color of H-scan changes as observed in the two example figures; the proportion of the blue scatterers increases with the growth of tumor for the both untreated and treated cases.

According to Figures 5, 6 and 7, H-scan trends for controls and treated groups are similar, but the increase is extended out over the longer lifespan of mice

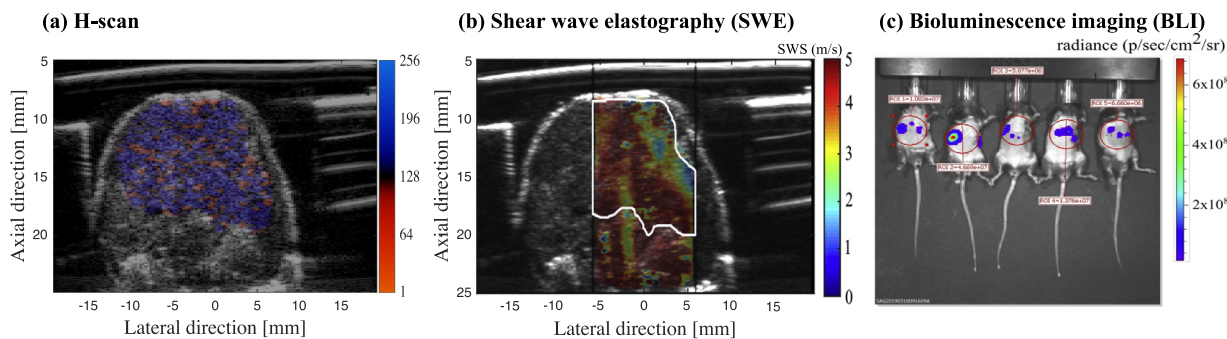


Fig. 3. (a) H-scan, the colormap shows relative size of scatterers; more blue and red colors represent relatively smaller and larger scatterers, respectively. (b) shear wave elastography (SWE) with color showing shear wave speed. (c) bioluminescence imaging (BLI) showing radiance.

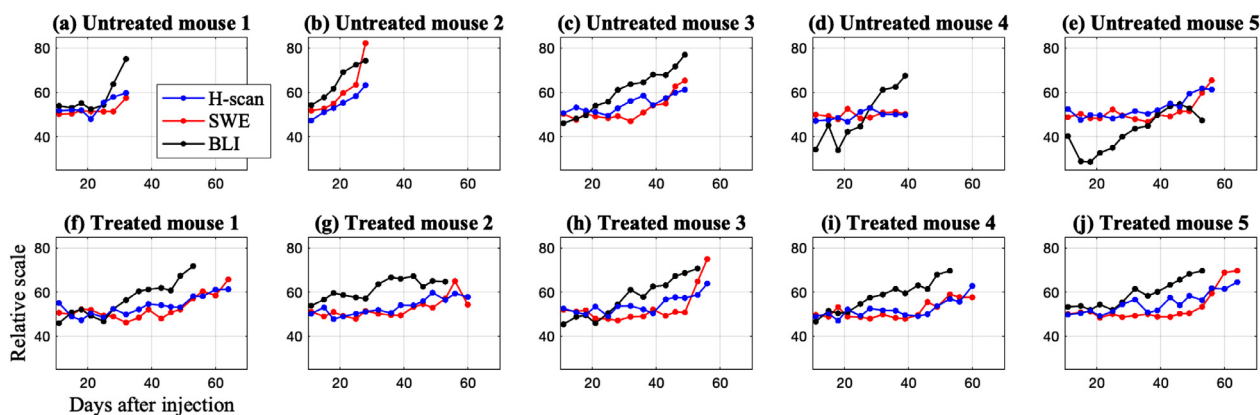


Fig. 4. The measurements of H-scan, shear wave elastography (SWE), and bioluminescence imaging (BLI) in 10 mice up to their death: percent of blue, SWS, and radiance, respectively. The three types of measurements are scaled relatively. The top row of (a–e) shows results from the untreated group, and the bottom row of (f–j) shows the results from the gemcitabine-treated group, which survived longer than the untreated group.

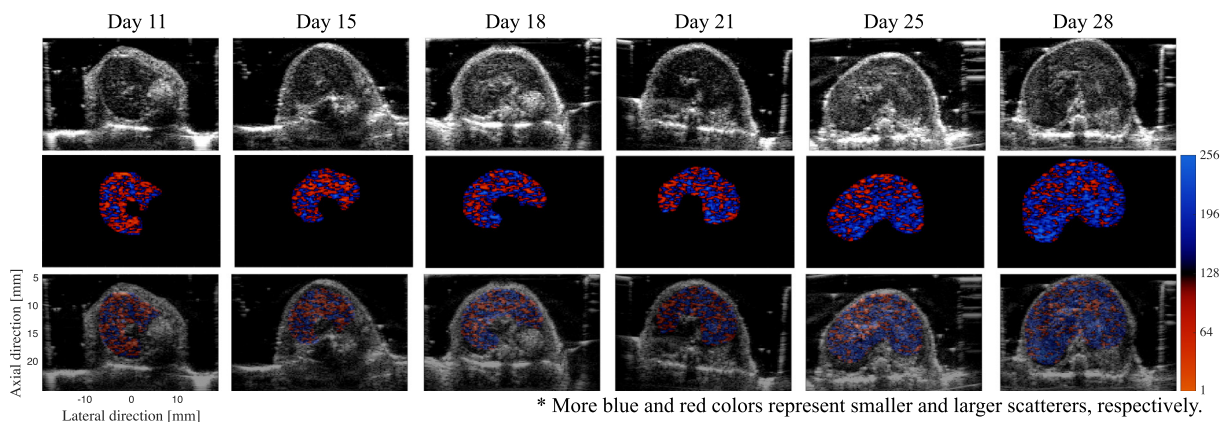


Fig. 5. B-scan (top row), H-scan colormap (middle row), and H-scan (bottom row) images for a mouse in the control untreated group at each time point. The liver boundary was manually segmented, which is used for H-scan processing. As the tumor grows over time, the H-scan colormap becomes more blue.

receiving chemotherapy. All of the mice in the untreated group died earlier than those in the treated group since the tumor growth rate is faster without the therapy, which is shown in Figures 4, 5 and 6. In Figure 4, the

slopes of the three measured lines for the untreated group are greater than those of the treated group. H-scan, in other words, can illustrate the increase in metastatic cancer with color regardless of the tumor growth rate.

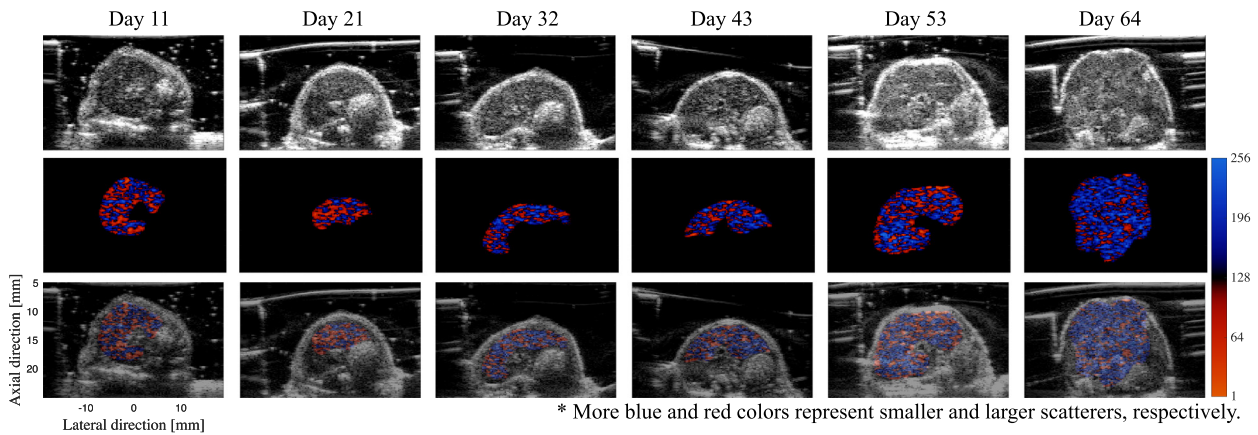


Fig. 6. B-scan (top row), H-scan colormap (middle row), and H-scan (bottom row) images for a mouse in the chemotherapy group at selected time points. As the tumor grows over time, the H-scan colormap becomes more blue.

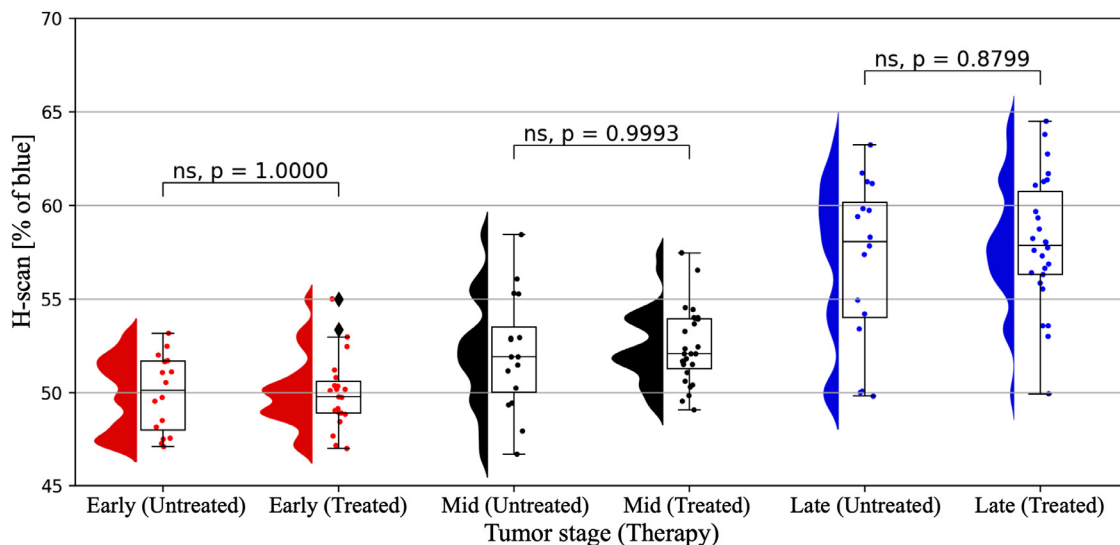


Fig. 7. Chemotherapy dependency for H-scan. H-scan results are not affected by whether the mice undergo treatment or not, which does not show significant difference for all tumor phases: early, mid and late tumor ("ns" indicates no significance).

The mice in this study were investigated from 11 d after tumor injection until their demise. To adjust for the different rates of growth and lifespans of the treated and untreated groups, the lifetime of each mouse was divided into three equal periods, which can be considered early, mid and late phases of the metastatic cancer growth. In Figure 7, the two groups of untreated and treated mice were compared at the defined tumor phases, demonstrating that there is no statistically significant difference between untreated mice and those undergoing therapy at similar tumor growth stages. The  $p$  values comparing the two groups are 1.0000, 0.9993 and 0.8799 for the early, mid and late phase tumors, respectively.

Since BLI is a standard assessment tool for quantifying tumor burden using the measurement of radiance,

H-scan results are compared with the radiance, as shown in Figure 8. The small scatterer percentage as a measurement of H-scan tends to increase consistently with the growth of radiance values. The Spearman's correlation analysis between H-scan and radiance was accomplished for all data and high burden tumor cases in Figures 8a and 8b, respectively. The two methods have statistically significant correlation with a Spearman's correlation of 0.61 for all data, including low burden tumor. When considering around 50% of high burden tumor cases based on radiance value, it shows stronger correlation ( $r_s = 0.724$ ).

Early, mid and late phases of tumor have three types of measured values by BLI, H-scan, and SWE, which are radiance, percentage of blue, and SWS, respectively; the

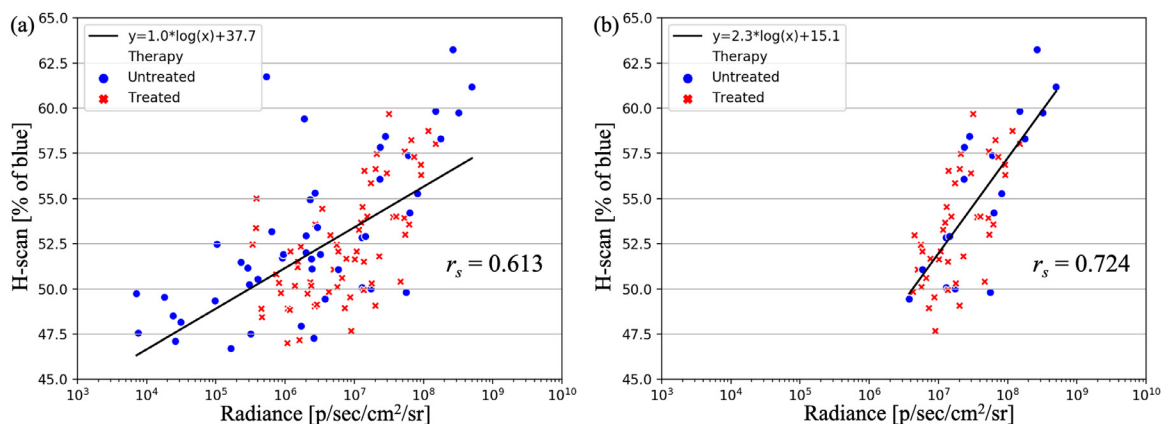


Fig. 8. A statistically significant correlation was shown between bioluminescence imaging (BLI) and H-scan. The Spearman's correlation is 0.613 and 0.724 for (a) all data and (b) high-burden tumor (radiance  $> 3.5 \times 10^6$ ), respectively. Linear fits are shown for reference only.

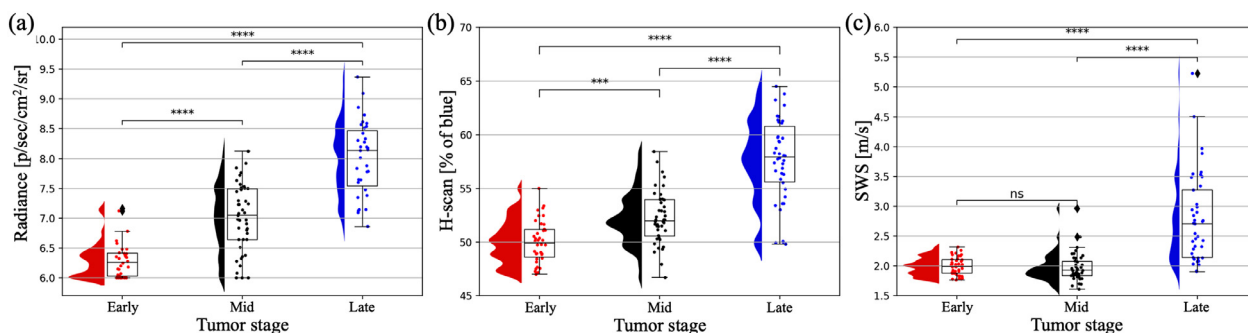


Fig. 9. Half violin and box plots for (a) radiance of bioluminescence imaging (BLI), (b) blue percent of H-scan and (c) shear wave speed (SWS) of shear wave elastography (SWE). The ten mice were investigated from 11 d post-implantation until their death, and each lifetime is divided into three groups: early, mid-, and late-phase metastatic cancer growth. The following notations for  $p$  value are used: ns (no significance),  $p > 0.05$ ; \*,  $p < 0.05$ ; \*\*,  $p < 0.01$ ; \*\*\*,  $p < 0.001$ ; \*\*\*\*,  $p < 0.0001$ .

results are depicted in Figure 9. Using the radiance and percentage of blue values, BLI and H-scan can differentiate the three tumor stages: early, mid and late. These show a statistically significant difference, when comparing the phases of tumor: early and mid; early and late; and mid and late. Comparison of radiance in Figure 9a shows  $p$  values of less than 0.0001. For H-scan in Figure 9b, when comparing the late-phase group with early and mid,  $p$  values are less than 0.0001; although the  $p$  value between early and mid is 0.0008, which is relatively greater than that of radiance, the  $p$  value of less than 0.001 can still indicate significant difference. As shown in Figure 9c, SWE also differentiates late-phase tumors from early and mid-phases consistently with previous results of BLI and H-scan. However, SWE does not show a significant difference between early and mid-phase tumors, of which the  $p$  value is 0.9832.

To evaluate the H-scan performance during the growth of tumors over time, we investigated raw data

with scatter plots in Figure 10. According to the comparison between Figures 10a and 10b, H-scan results tend to more consistently increase as the radiance increases; however, SWS estimation is likely to remain relatively constant at low and mid radiance, while rapidly increasing at high radiance range. At the smaller measurement values by H-scan and SWE in Figure 10c, SWS results are hardly changed when those of H-scan increase. There appears to be a more robust correlation between BLI and H-scan compared with that between SWS and the others, since SWS has less consistent results at early to mid-stage of tumor growth.

H-scan performance was further assessed quantitatively using a Spearman's correlation analysis in Figure 11. For high-burden tumor, three methods show comparable results with similar Spearman's correlation values around 0.7: 0.7239 for BLI and H-scan; 0.6659 for BLI and SWE; and 0.6920 for H-scan and SWE. However, when considering all data, including low-burden tumor, H-scan and BLI have stronger correlation,

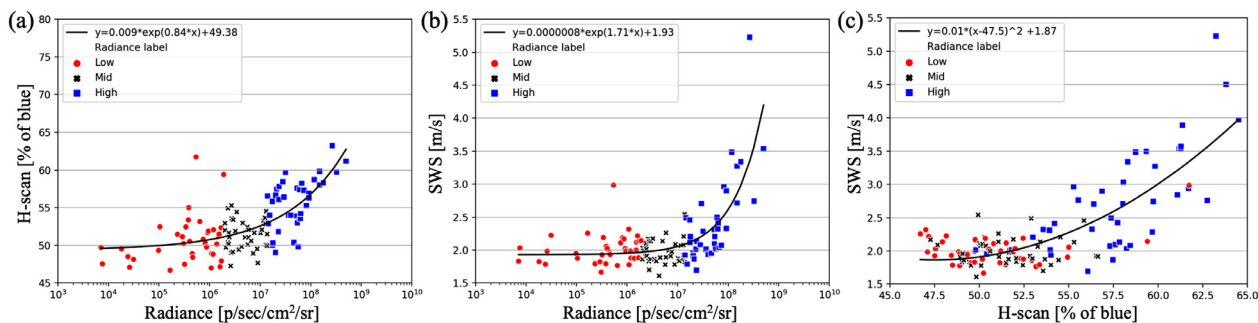


Fig. 10. Scatter plots between the methods: (a) bioluminescence imaging (BLI) and H-scan; (b) BLI and shear wave elastography (SWE); (c) H-scan and SWE. Nonlinear fits are shown for visual reference only.

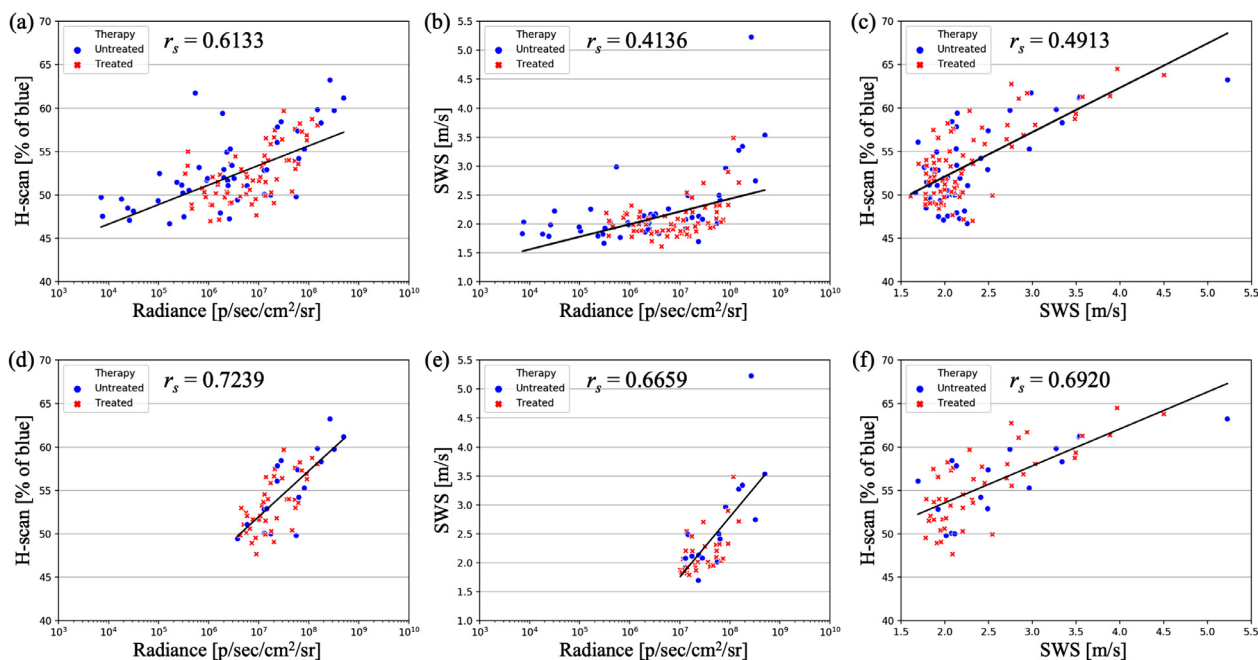


Fig. 11. Spearman's correlation between the three methods: (a) and (d) bioluminescence imaging (BLI) and H-scan; (b) and (e) BLI and shear wave elastography (SWE); (c) and (f) H-scan and SWE. To calculate the Spearman's correlation, the upper row used all investigated data including low burden tumor. The lower row used high burden tumors with radiance greater than  $3.5 \times 10^6$ ,  $10^7$ ,  $7 \times 10^7$  for (d), (e), and (f), respectively; the threshold values are determined to maximize  $r_s$  for each comparison. Linear fits are shown for reference only.

with a coefficient of 0.6133, than the correlation including SWE, which is compared with BLI and H-scan with Spearman's coefficients of 0.4136 and 0.4913, respectively.

### DISCUSSION

The PDAC metastatic model results in a progressive increase in tumor burden, leading to death (Soares et al. 2014). To evaluate the role of H-scan in assessing metastatic tumor growth in the liver, we compared different imaging modalities: BLI, H-scan, and SWE. BLI (Rehemtulla et al. 2000) is based on photon emissions that generally grow with increasing

tumor burden. It requires injecting luminous material for imaging. On the other hand, SWE and H-scan are non-invasive methods, but SWE requires generation of acoustic radiation force in addition to the B-scan imaging procedure, and can result in lowering of the imaging frame rate, which is a drawback for real-time imaging ultrasound. However, H-scan does not require any change in the transmission procedure from B-scan. H-scan uses RF or IQ data during conventional B-mode imaging and only requires appropriate post-processing. As such, it does not affect the frame rate, which is important since real-time imaging is a prominent advantage of ultrasound compared to other imaging modalities.

BLI and SWE have different limitations for imaging deep regions: BLI penetration is limited by optically attenuating and scattering overlying tissues, whereas SWE is limited in terms of the depth of focus because of attenuation of the push pulse. However, the H-scan is applicable to the depth at which the noise floor of the imaging pulse is encountered.

Considering the performance of BLI, it is reported that it has excellent correlation with magnetic resonance imaging for measurement of tumor volume (Rehemtulla *et al.* 2000). One limitation of this study and a topic for future research is a relative comparison of H-scan, SWE, and BLI against additional sensitive modalities, including positron emission tomography and ultrasound contrast studies. For example, a study of targeted contrast agents for colorectal cancer metastases in a liver model found greater detection of small lesions with contrast compared with BLI (Hackl *et al.* 2016). A future multi-modality cross-comparison would help to distinguish the relative advantages and complexities of each approach for detecting small lesions within the liver and assessing tumor burden.

Although H-scan and SWE are both related to structural components of tissue, the results of BLI and H-scan show comparable accuracy for differentiating tumor phases. They show better performance for early phase tumor imaging than SWE, which did not show a significant difference between early and mid-phase metastatic cancer in the liver. Therefore, H-scan can be more sensitive and yet simpler in terms of transmission sequencing than SWE for this application.

## CONCLUSION

All three of the imaging-based analyses (shear wave, H-scan, and bioluminescence) trended toward increasing measures with time during the progressive growth of the PDAC metastases in the liver. The measured increases over time were delayed for the group receiving chemotherapy, yet achieved significantly higher values near the end stage, leading to death in both treated and untreated groups. This result suggests that the ultrasound-based analyses can track the progression of tumor burden or its delay following therapies. Furthermore, the comparison of early to mid-phase metrics indicated that H-scan had a sensitivity that was significant and comparable to the bioluminescent measures. These results are promising for the early characterization of responders and the monitoring, over time, of cancer progression.

*Acknowledgments*—This work was supported by National Institutes of Health grants R21 EB025290 and R56 EB024320.

*Conflict of interest disclosure*—The authors declare that they have no conflict of interests.

## REFERENCES

- Ahmed R, Gerber SA, McAleavey SA, Schifitto G, Doyley MM. Plane-wave imaging improves single-track location shear wave elasticity imaging. *IEEE Trans Ultrason Ferroelectr Freq Control* 2018;65:1402–1414.
- Ahmed R, Ye J, Gerber SA, Linehan DC, Doyley MM. Preclinical imaging using single track location shear wave elastography: Monitoring the progression of murine pancreatic tumor liver metastasis *in vivo*. *IEEE Trans Med Imaging* 2020;39:2426–2439.
- Barr RG, Nakashima K, Amy D, Cosgrove D, Farrokh A, Schafer F, Bamber JC, Castera L, Choi BI, Chou YH, Dietrich CF, Ding H, Ferraioli G, Filice C, Friedrich-Rust M, Hall TJ, Nightingale KR, Palmeri ML, Shiina T, Suzuki S, Sporea I, Wilson S, Kudo M. WFUMB guidelines and recommendations for clinical use of ultrasound elastography: Part 2: Breast. *Ultrasound Med Biol* 2015;41:1148–1160.
- Chang JM, Park IA, Lee SH, Kim WH, Bae MS, Koo HR, Yi A, Kim SJ, Cho N, Moon WK. Stiffness of tumours measured by shear-wave elastography correlated with subtypes of breast cancer. *Eur Radiol* 2013;23:2450–2458.
- Dizeux A, Payen T, Le Guillou-Buffello D, Comperat E, Gennisson JL, Tanter M, Oelze M, Bridal SL. *In vivo* multiparametric ultrasound imaging of structural and functional tumor modifications during therapy. *Ultrasound Med Biol* 2017;43:2000–2012.
- Fernandes J, Sannachi L, Tran WT, Koven A, Watkins E, Hadizad F, Gandhi S, Wright F, Curpen B, El Kaffas A, Faltny J, Sadeghi-Naini A, Czarnota G. Monitoring breast cancer response to neoadjuvant chemotherapy using ultrasound strain elastography. *Transl Oncol* 2019;12:1177–1184.
- Hackl C, Schacherer D, Anders M, Wiedemann LM, Mohr A, Schlitt HJ, Stroszczyński C, Tranquart F, Jung EM. Improved detection of preclinical colorectal liver metastases by high resolution ultrasound including molecular ultrasound imaging using the targeted contrast agent BR55. *Ultraschall Med* 2016;37:290–296.
- Khairalseed M, Hoyt K, Ormachea J, Terrazas A, Parker KJ. H-scan sensitivity to scattering size. *J Med Imaging (Bellingham)* 2017;4:043501.
- Khairalseed M, Javed K, Jashkaran G, Kim JW, Parker KJ, Hoyt K. Monitoring early breast cancer response to neoadjuvant therapy using H-scan ultrasound imaging: Preliminary preclinical results. *J Ultrasound Med* 2019;38:1259–1268.
- Li F, Huang Y, Wang J, Lin C, Li Q, Zheng X, Wang Y, Cao L, Zhou J. Early differentiating between the chemotherapy responders and nonresponders: Preliminary results with ultrasonic spectrum analysis of the RF time series in preclinical breast cancer models. *Cancer Imaging* 2019;19:61.
- Mills BN, Connolly KA, Ye J, Murphy JD, Uccello TP, Han BJ, Zhao T, Drage MG, Murthy A, Qiu H, Patel A, Figueroa NM, Johnston CJ, Prieto PA, Egilmez NK, Belt BA, Lord EM, Linehan DC, Gerber SA. Stereotactic body radiation and interleukin-12 combination therapy eradicates pancreatic tumors by repolarizing the immune microenvironment. *Cell Rep* 2019;29:406–421.e5.
- Parker KJ. Attenuation measurement uncertainties caused by speckle statistics. *J Acoust Soc Am* 1986;80:727–734.
- Parker KJ. The H-scan format for classification of ultrasound scattering. *J OMICS Radiol* 2016a;5:1000236.
- Parker KJ. Scattering and reflection identification in H-scan images. *Phys Med Biol* 2016b;61:L20.
- Parker KJ. The first order statistics of backscatter from the fractal branching vasculature. *J Acoust Soc Am* 2019;146:3318–3326.
- Parker KJ, Baek J. Fine-tuning the H-scan for discriminating changes in tissue scatterers. *Biomed Phys Eng Express* 2020;6:045012.
- Parker KJ, Doyley MM, Rubens DJ. Imaging the elastic properties of tissue: The 20 year perspective. *Phys Med Biol* 2011;56:R1–R29.
- Parker KJ, Waag RC. Measurement of ultrasonic attenuation within regions selected from B-scan images. *IEEE Trans Biomed Eng* 1983;30:431–437.
- Rehemtulla A, Stegman LD, Cardozo SJ, Gupta S, Hall DE, Contag CH, Ross BD. Rapid and quantitative assessment of cancer

- treatment response using *in vivo* bioluminescence imaging. *Neoplasia* 2000;2:491–495.
- Sannachi L, Gangeh M, Tadayyon H, Gandhi S, Wright FC, Slodkowska E, Curpen B, Sadeghi-Naini A, Tran W, Czarnota GJ. Breast cancer treatment response monitoring using quantitative ultrasound and texture analysis: Comparative analysis of analytical models. *Transl Oncol* 2019;12:1271–1281.
- Soares KC, Foley K, Olino K, Leubner A, Mayo SC, Jain A, Jaffee E, Schulick RD, Yoshimura K, Edil B, Zheng L. A preclinical murine model of hepatic metastases. *J Vis Exp* 2014;51677.
- Tadayyon H. Ultrasound imaging of apoptosis: Spectroscopic detection of dna-damage effects *in vivo*. In: Didenko VV, (ed). *Fast detection of DNA damage : Methods and protocols*. New York: Humana Publishing; 2017. p. 41–60.
- Tadayyon H, Sannachi L, Gangeh M, Sadeghi-Naini A, Tran W, Trudeau ME, Pritchard K, Ghandi S, Verma S, Czarnota GJ. Quantitative ultrasound assessment of breast tumor response to chemotherapy using a multi-parameter approach. *Oncotarget* 2016;7:45094–45111.
- Turco S, El Kaffas A, Zhou J, Wijkstra H, Willmann JK, Mischi M. Quantitative ultrasound molecular imaging for antiangiogenic therapy monitoring. 2016 IEEE International Ultrasonics Symposium (IUS). 1–4. doi: 10.1109/ULTSYM.2016.7728653 <https://ieeexplore.ieee.org/document/7728653>
- Zhou J, Zhang H, Wang H, Lutz AM, El Kaffas A, Tian L, Hristov D, Willmann JK. Early prediction of tumor response to bevacizumab treatment in murine colon cancer models using three-dimensional dynamic contrast-enhanced ultrasound imaging. *Angiogenesis* 2017;20:547–555.